estec
European Space Research and Technology Centre
Keplerlaan 1
221 AZ Noordwijk
The Netherlands

Responsible Technical Officer
Mr. Alan Owens (IPL-IS)
Tel. +31 7156 55326
Fax +31 7156 53854
E-mail: alan.owens@esa.int

ITT No. – AO/1-8070/14/F/MOS
ESA EXPRESS Procurement Plus – “EXPRO+”
Development of Graphene based THz
and X-Ray Radiation Detectors

Executive Summary Report (Public)

Version	Date	Status, Changes	Authors
1.1	November 10th, 2016	First version	Sanna Arpiainen, Juha Riikonen, Andrey Timofeev, Wonjae Kim, Markku Kainlauri, Hannu Ronkainen, Mika Prunnila, Juha Hassel

Table of Contents

LIST OF FIGURES

LIST OF TABLES

LIST OF ABBREVIATIONS

III-V	Three-five semiconductors
AC	Alternating current
AFM	Atomic force microscope
ALD	Atomic layer deposition
ASIC	Application-specific integrated circuit
CMM	Constant mobility model
CMOS	Complementary metal–oxide–semiconductor
CVD	Chemical vapour deposition
CW	Continuous wave
DC	Direct current
EBL	Electron beam lithography
EU	European Union
eV	Electron Volt
FET	Field effect transistor
GDEPFET	Graphene DEpleted P-channel Field Effect Transistor
GFET	Graphene Field Effect Transistor
HEMT	High-electron-mobility transistor
HR	High resistive
IR	Infrared
IV	Current-voltage
KID	Kinetic inductance detector
MOSFET	Metal oxide semiconductor FET
PIN	p-type / insulator / n-type
PTCVD	Photo-thermal CVD
RD	Reference document
RF	Radio frequency
RIE	Reactive ion etching
SD	Sentaurus Device
SEM	Scanning electron microscope
SoW	Statement of work
TCAD	Technology Computer Aided Design
TLM	Transfer length method
TN	Technical note
TRL	Technology readiness level

EXECUTIVE SUMMARY REPORT

This report first shortly reviews graphene based photodetection and device fabrication, then separately X-ray detection and THz detection.

1 GRAPHENE PHOTODETECTORS FOR VISIBLE & IR REGIME

In the first demonstrations, the detection of photons with graphene was based on the pn-junction generated by the graphene-metal contact. There the active detector area is a narrow line with length determined by the contact edge and as the absorption of photons incident to a single layer of graphene is 2.3 % at highest, the detector efficiency is rather modest. However, the detector has very high speed, demonstrated up to 40 GHz and predicted to reach over 500 GHz, possibly limited only by the contact resistance.[1]

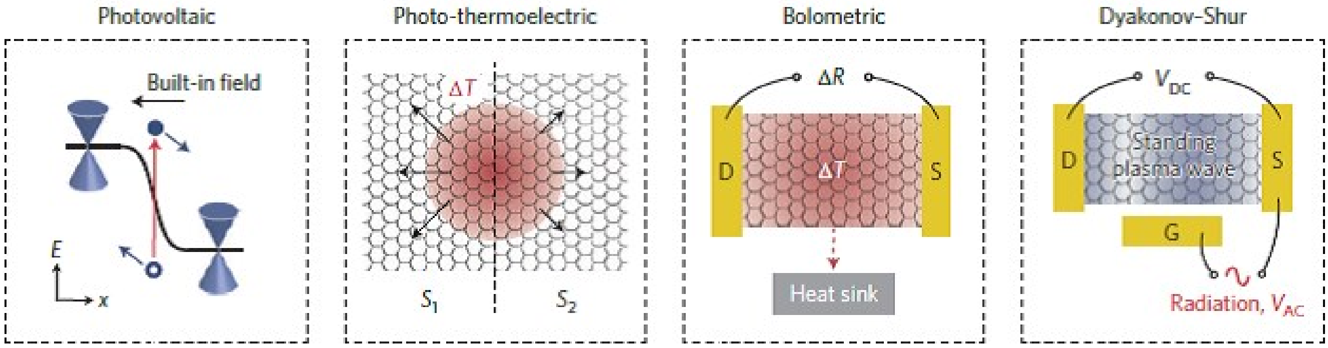

Figure 1.1 Schematic representation of the four photocurrent generation mechanisms discussed in TN1.1. First panel: electron–hole (solid and open circle) separation by an internal electric field. Second and third panels: red shaded area indicates elevated electron temperature with ΔT the temperature gradient and ΔR the resistance across the channel; S_1 and S_2, Seebeck coefficient in graphene areas with different doping. Third and fourth panels: S and D indicate source and drain, and G the gate; V_{DC}, photogenerated d.c. voltage; V_{AC}, a.c. voltage applied to the gate.[2]

The photocurrent generation in the metal-graphene-metal photodetectors is based on a photovoltaic effect presented in the first panel of **Figure 1.1**, where the photogenerated electron–hole (e–h) pairs are separated by built-in electric fields at junctions between positively (p-type) and negatively (n-type) doped regions of graphene or between differently doped sections. In semiconductors the same effect could be achieved by applying a source–drain bias voltage (V_{bias}), producing an external electric field, but this is not a good approach in the case of graphene, as it is a semimetal and therefore would generate a large dark current (leakage). Instead, the built-in field is typically introduced by taking advantage of the work-function difference between graphene and the contacting metals.[3] The doping of graphene in the contacted area is fixed by the metal and typically p-type for metals with a work function higher than that of intrinsic graphene (4.45 eV), whereas the graphene channel can be adjusted to p- or n- state by the gate. The photocurrent direction depends only on the direction of the electric field, not on the overall doping level. Thus, it switches sign when going from p–n to n–p, or from p–p+ to p+–p, where p+ means stronger p-type doping compared with p.[2]

In graphene, electron–electron (e–e) scattering[4] can lead to the conversion of one high-energy e–h pair into multiple e–h pairs of lower energy[5]. This carrier multiplication process can potentially enhance the overall photodetection efficiency.[2]

Other than photovoltaic panels in Figure 1.1 refer to the mechanisms employed in the terahertz detection (and panel “photo-thermoelectric” in some cases IR and optical frequencies) and are described in Section 4 in more detail.

Various techniques and phenomena have been developed and employed to improve the light-matter interaction in graphene based photodetectors. One of the simplest ideas is to increase the interaction time by placing graphene detector into a node of an optical cavity, thus increasing the light coupling into graphene to up to 60%, but with the cost of the bandwidth. Coupling can also be increased by placing graphene on top of a waveguide, providing an optical mode parallel to graphene; an interaction length of a few tens of microns was found to be able to modulate the optical mode with 3 dBm up to 1 GHz.[6] This technology has high prospects in optical signal processing, for example in optical data links, as the current alternatives for fast modulation are far too expensive.

The light-matter interaction has also been enhanced with e.g. multilayer graphene, and in heterostructures employing nanostructure induced plasmon resonance[7] or charge transfer from quantum dots, resulting in an efficient photogating[8]. Another approach is to employ the hot carrier multiplication (Auger processes) by fast separation of the electron – hole pairs.[9] Recently, the wide band absorption efficiency of the detection has been improved by vertical tunnelling structure to extract the hot photogenerated carriers into another graphene layer through a thin insulating barrier.[10]

Table 1.1 Performance parameters of graphene and related materials based photodetectors.[2]

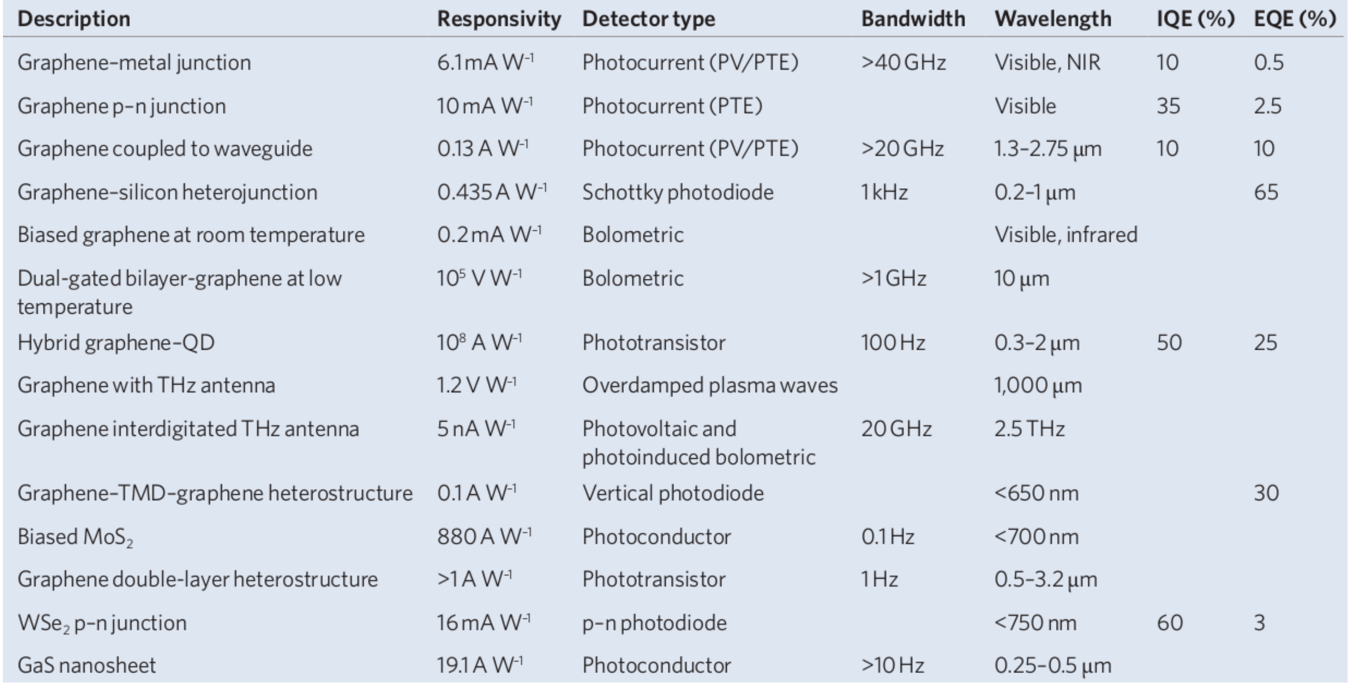

Description	Responsivity	Detector type	Bandwidth	Wavelength	IQE (%)	EQE (%)
Graphene–metal junction	6.1 mA W^{-1}	Photocurrent (PV/PTE)	>40 GHz	Visible, NIR	10	0.5
Graphene p–n junction	10 mA W^{-1}	Photocurrent (PTE)		Visible	35	2.5
Graphene coupled to waveguide	0.13 A W^{-1}	Photocurrent (PV/PTE)	>20 GHz	1.3–2.75 μm	10	10
Graphene–silicon heterojunction	0.435 A W^{-1}	Schottky photodiode	1 kHz	0.2–1 μm		65
Biased graphene at room temperature	0.2 mA W^{-1}	Bolometric		Visible, infrared		
Dual-gated bilayer-graphene at low temperature	10^5 V W^{-1}	Bolometric	>1 GHz	10 μm		
Hybrid graphene–QD	10^8 A W^{-1}	Phototransistor	100 Hz	0.3–2 μm	50	25
Graphene with THz antenna	1.2 V W^{-1}	Overdamped plasma waves		1,000 μm		
Graphene interdigitated THz antenna	5 nA W^{-1}	Photovoltaic and photoinduced bolometric	20 GHz	2.5 THz		
Graphene–TMD–graphene heterostructure	0.1 A W^{-1}	Vertical photodiode		<650 nm		30
Biased MoS_2	880 A W^{-1}	Photoconductor	0.1 Hz	<700 nm		
Graphene double-layer heterostructure	>1 A W^{-1}	Phototransistor	1 Hz	0.5–3.2 μm		
WSe_2 p–n junction	16 mA W^{-1}	p–n photodiode		<750 nm	60	3
GaS nanosheet	19.1 A W^{-1}	Photoconductor	>10 Hz	0.25–0.5 μm		

2 GRAPHENE GROWTH AND PROCESSING

The most important aspect in graphene based detector commercialization is the scale-up of the graphene device fabrication to enable the wafer-level production of high mobility devices that is the key to the increased sensitivity in both X-ray and THz detection.

The current consensus in graphene production is that the large-area high quality (semiconductor grade) graphene will be based on chemical vapour deposition (CVD) on catalytic surfaces, such as copper or platinum, and subsequent transfer to the preferred substrate. Graphene production at wafer level is also done with sublimation based growth on SiC, which is a promising method for applications where the high cost of the substrate is not an issue.

The current challenges in graphene production are in the material homogeneity and topology; wrinkles originating from the different thermal expansion coefficients of the catalytic template and graphene, wide grain boundaries opening into copper films during or after growth and transferring into voids in graphene and, when avoiding those with the use of copper foils, the relatively high topology of the foils compared to silicon wafers smoothness, causing problems in transfer.

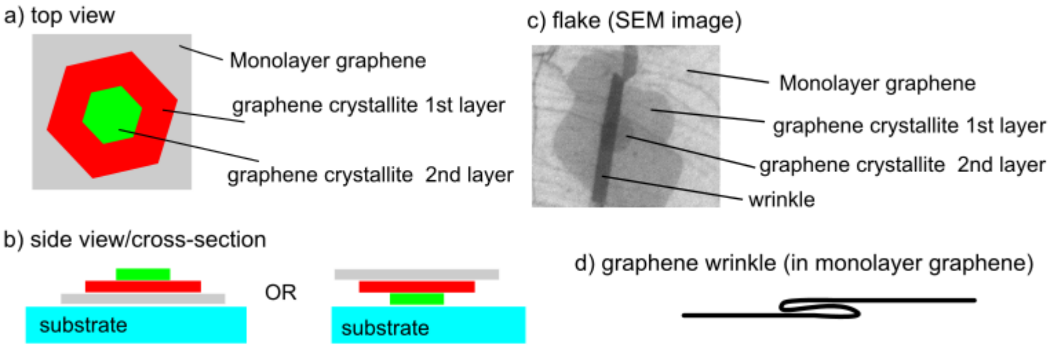

Figure 2.1 Schematic of graphene flakes (crystallites) on monolayer graphene: a) top view b) side view. c) SEM image of a graphene flake and d) side view schematic of a wrinkle.

In general, the challenge of the transfer of large-area graphene from the catalytic surface to the target substrate has been solved in several laboratories and small companies producing large area graphene for the market, with solutions ranging from dry transfer to wet transfer with advanced surface cleaning techniques. Due to the complexity and dedication required for high quality transfer, the use of commercial graphene wafer supplies should be seen as the first option in small and medium scale graphene device production.

2.1 Commercially available graphene sheets

Graphene was acquired from three different suppliers: **SP1** (Europe), **SP2** (USA) and **SP3** (Asia). Suppliers did not give any guarantee for the sample quality and at the moment there are no standard specifications for graphene samples. The samples were purchased as high-quality monolayer graphene fabricated by CVD. Graphene was transferred on SiO_2/Si substrates by the suppliers. Several samples were used from each supplier during the characterization.

The samples were analysed both structurally and electrically. SEM images bilayer crystallites (islands) in all samples. Diameter of the flakes is about 0.5-1 μm and areal density is approximately the same for all samples. In addition to flakes, all samples have wrinkles. In some random locations SEM imaging revealed also voids (holes) in the graphene films, but there was no significant difference in the samples from different suppliers. The **SP3** showed charging during the SEM imaging, possibly originating for example polymer residues from the transfer process.

All samples display typical Raman fingerprint for high-quality monolayer graphene, but the spectrum measured from the **SP3** sample the crystalline quality was the highest and defect density was the lowest among the suppliers.

The main electrical characteristic of graphene (mobility, sheet resistance, contact resistance, intrinsic doping and Dirac point) were obtained from electrical transport measurements utilizing transfer length method (TLM) and constant mobility model (CMM). All commercial graphenes showed pretty similar electrical performance, with mobilities in the range of 2 000 cm^2/Vs and intrinsic carrier concentrations of about 10^{12} cm^{-2}. There were no significant differences in the contact resistance, which varied between 400 to 1700 Ω.

These are not state-of-the-art values for CVD graphene, but it can be described as a typical, good values. Samples from different suppliers cannot be discriminated based on their electrical characterization. However, structurally, and from the point of view of intrinsic doping, the materials were different. All samples contained multi-layered areas (flakes) but with different characteristics.

2.2 Device processing

In addition to the graphene quality, the electrical characteristics are strongly influenced by the atomic level smoothness, trapped charges and other properties (phonon frequencies, polarizability) of the substrate and of the top dielectric, which makes the material selections crucial for the device performance. The best results with respect to charge carrier mobility have been obtained by sandwiching graphene between the atomically smooth *h*-BN films, reaching 70 000 cm^2/Vs at room temperature. However, this technique is yet not available for large-scale production, but is limited by the size of the exfoliated hBN flakes.

Besides the material selection, the amount of interface charges is affected by the transfer and cleaning techniques. This is the most difficult part of the process sequence to monitor, stabilize and optimize because of the multitude of different processes involved. This is also one of the major sources of wafer scale inhomogeneity.

In addition, contact resistance is one of the most relevant development targets in graphene processing, and a major source of parasitic effects in all high frequency applications, including THz detection. Most promising methods are linked to the optimization of the edge area of graphene inside the contacts, including 1D edge contacts. In general, all contacting methods are scalable to any wafer size.

To achieve e.g. the mobility of 5000 cm^2/Vs theoretically required for high performance THz detection as described later in this document, *h*BN or other exotic substrates are not required, but the purity of graphene surface and the smoothness of the standard dielectric substrates are essential. Such mobilities are often obtained in Aalto and VTT in device processing,[11] but unfortunately not routinely achieved in new device concepts and require process-related optimization. This was not possible within the cost-frame of this project, but can be easily achieved when the budget allows a few iterations.

3 X-RAY DETECTION

3.1 GFET detector with absorbing substrate

The device concept of the graphene GFET for radiation detection is based on utilizing non-conductive absorber substrate as illustrated in **Figure 3.1**b. When the gate voltage is applied the voltage is essentially across the whole structure as shown in Figure 3.1c (low field case). However, as the radiation ionizes charges within the absorber, the conductivity of the absorber substrate is increased and the gate voltage is now across the thin insulator layer (high field case in Figure 3.1d). The transient change of the effective gate voltage for the graphene channel is detected as a relative change of the resistivity of the GFET as described by the analytic model below.

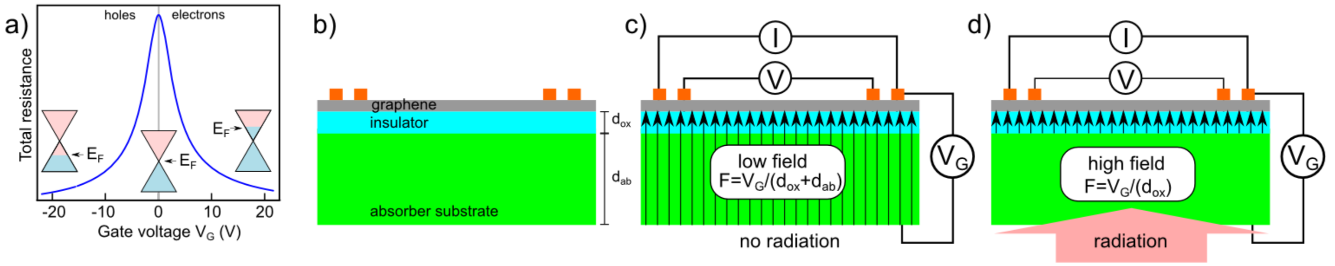

Figure 3.1 a) Fermi level shift as function of gate voltage in a GFET. b) Schematic of the GFET radiation detector. c) Operation of the GFET when no radiation is applied and the electric field is across the whole absorber substrate (low field). d) As the radiation increases the conductivity of the absorber substrate via ionization, the gate voltage is across only the thin insulator layer (high field).

To optimize the sensitivity of graphene, the relative change of the resistivity as a function of the gate voltage should be maximized. For graphene, there are two main ways. First is the optimization of the graphene quality, processing and device fabrication. Secondly, it is rather crucial for the detector sensitivity that the operation point is at Dirac point (**Figure 3.2**a); only a minor change in the gate voltage can induce significant change in the resistance. In addition to the fabrication related methods listed above, an additional top gate electrode enables configuration of the Dirac point of the graphene channel. Moreover, it is an active method and it is viable during the device operation.

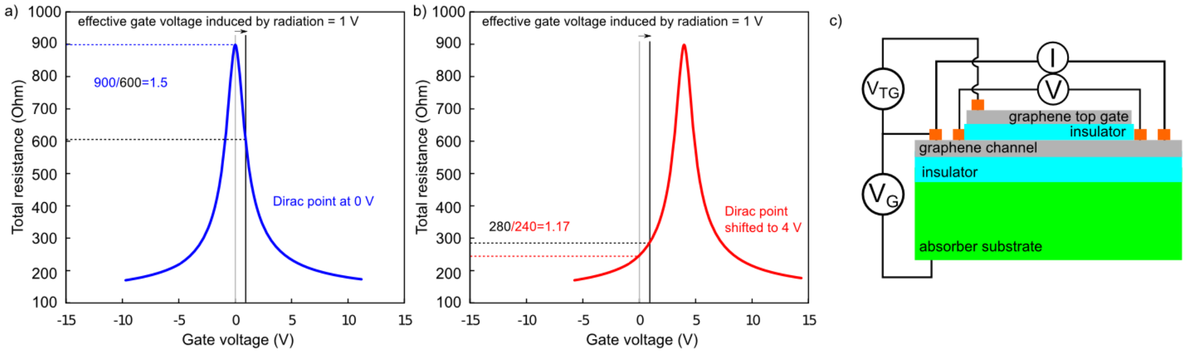

Figure 3.2 Effect of the Dirac point shifting to the detector sensitivity. Assuming that effective radiation induced gate voltage shift is 1 V in this example, a) Dirac point at V_G=0 V would results in relative change in graphene resistance to be ~50 %. b) For a device with a Dirac point shifted to 4 V the change is only ~17 %. c) Illustration of a GFET with additional top gate electrode fabricated from graphene to enable top gate control of the Dirac point. Graphene as a transparent electrode does not oppose the limitations as opaque metal electrode would.

The relatively high energy of the soft X-ray radiation allows the selection of absorbing material with band gap well above k_BT at room temperature. Compared to the visible light, the absorption coefficients are typically much smaller with X-ray, but the amount of generated carriers for each photon is typically significant. In the case of silicon, VTT is currently initializing cleanroom infrastructure modification to facilitate full radiation detector process flow on 1 mm thick silicon wafers in order to increase the absorbance of the silicon substrate in soft X-ray radiation detection to the level required in medical imaging. Silicon is also commonly used in X-ray and particle detection in high flux applications, where the thinned absorber allows for continuous flux through the detector.

When considering integration with graphene, silicon is the standard substrate in graphene electronics, with generally acceptable influence on the electronic structure and transport in graphene. Larger band gap materials like SiC and CdTe would allow room temperature operation of the GFET detectors [**RD5**]. In addition, graphene can be synthesized directly on the SiC using a thermal evaporation technique[12]. However, GFETs on SiC and CdTe do not show well confined Dirac peaks [**RD5**, Ref. 13]. Therefore these materials are problematic as absorbers for GFET radiation detectors relying on the response of the Fermi level to small changes in the electric field.

Graphene based X-ray detectors have been demonstrated based on the device architecture and operational functionality described above [**RD1-RD7**]. Variation in X-ray energy and flux was reported to correlate to changes in the resistance in graphene.[13] Furthermore, the authors observed more that 50% change in the resistance between the high (40 keV, 80 µA) and low (15 keV, 15 µA) X-ray flux at 4.3 K, but received no signal at room temperature due to the conductivity of the silicon substrate. In SiC-based devices they observed an about 70% change in graphene resistance with X-ray irradiation also at room temperature. In this study[13] Koyabsi *et al.* also note that the GFET based detector is also viable for detecting visible light underlining that the basic device performance and overall functionality of the device architecture can be determined using visible light source.

3.2 Depleted p-channel FET structure

Change in the electric field distribution in the semiconducting absorber gate of the graphene FET induces the desired change in conductivity of the graphene channel. However, in the absence of charge removal mechanism between the sampling processes, the irradiation generated carriers accumulate as charges under the gate dielectric. Charges accumulated from the previous irradiation are trapped at the semiconductor-insulator interface and it may take hours to drain these charges away [**RD5**]. The sensitivity of the graphene gate is significantly degraded since charges induced by next radiation event will be added to the existing ones causing the operation of graphene gate moving away from the Dirac point. Although short reversed (opposite) pulse can be used to enhance the recovery time [**RD5**] it is not a practical way to improve the detector dynamics due to the increased complexity of the readout and control electronics and the time required for stabilization. In this simple device, also the intrinsic carriers in the non-depleted semiconductor induce dark conductivity in the gate, thus decreasing the contrast to the radiation event. Therefore, further improvements are required to address the detector sensitivity and recovery time especially when targeting energy dispersive spectroscopy.

Graphene DEPFET [**RD5, RD6**] is an intriguing alternative as already stated in the SOW. **Figure 3.3**a shows a proposed structure of graphene DEPFET. A p-channel field effect transistor is placed on the fully depleted bulk, allowing the use of lower quality semiconductor absorbers. The highly doped region underneath the transistor channel forms an internal gate where the potential stays at maximum. Electrons induced anywhere in the depleted bulk are collected to the potential maximum inducing mirror charges in the channel. These accumulated charges change the electric field under the insulator which is sensed by the graphene gate. After readout, the induced charges in the channel can be drained out by switching on the clear mechanism. As a result, the detector is reset for a detection of a new radiation event.

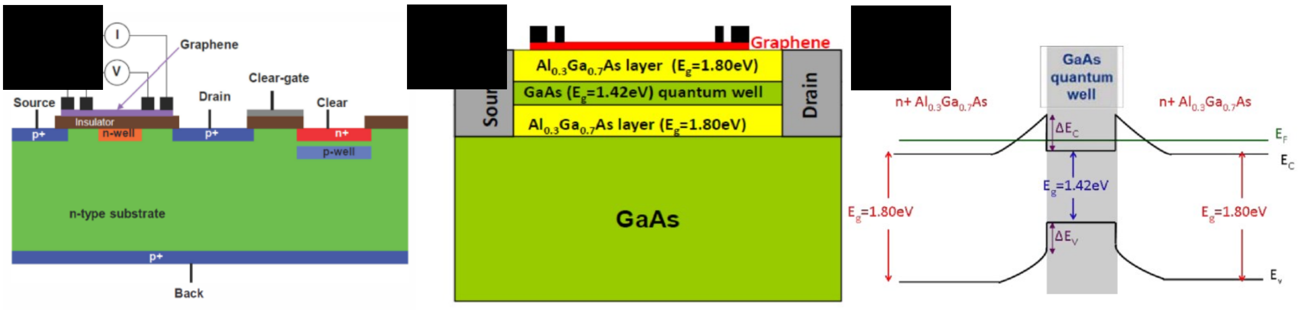

Figure 3.3 a) Device structure for GDEPFET on silicon. [RD5] b) Device structure of a GFET based on GaAs as an absorber substrate and a near-surface AlGaAs/GaAs quantum well as a spatial confinement for the carrier. Lateral drain-source contacts allow the rapid and efficient depletion of the carriers. c) Schematic band diagram of the quantum well device structure.[13]

GaAs based device structures might provide an alternative pathway to achieve same operational functionality as in DEPFETs. **Figure 3.3**b-c depicts a recently proposed GFET detector structure, which utilized near-surface AlGaAs-GaAs quantum well as a confinement for carriers induced by the radiation in the GaAs absorber substrate[13].

3.3 X-Ray detector demonstrator and simulations

To investigate the limits of the room-temperature X-ray detection with silicon absorber, the substrates were fabricated on state-of-the-art X-ray detector process developed at VTT. The measured minority carrier lifetime in n-type wafers before graphene processing was 3.5 ms.

Graphene field-effect transistors (GFETs) were fabricated by transferring graphene on the pre-processed absorber substrates. Components with unprotected graphene exposed to ambient were been fabricated in Aalto University using electron beam lithography (EBL) based process, and components with Al_2O_3 coated graphene with optical lithography based process at VTT. The advantage of the uncovered graphene components is the higher mobility, whereas the coated components are more stable in ambient conditions. Al_2O_3 coating also serves as a top dielectric, which is required for further fabrication of top gate to allow adjusting the most sensitive operation points of graphene and silicon absorber.

The detectors were measured in dark and while exposing to soft x-ray irradiation and to visible light in ambient lightning at approximately 500 lx (**Figure 3.4**). The AMPTEK Mini-X with an Ag anode was used as the soft x-ray source. The GFET channel resistance showed only minor response to the light, and practically no response to the soft X-rays.

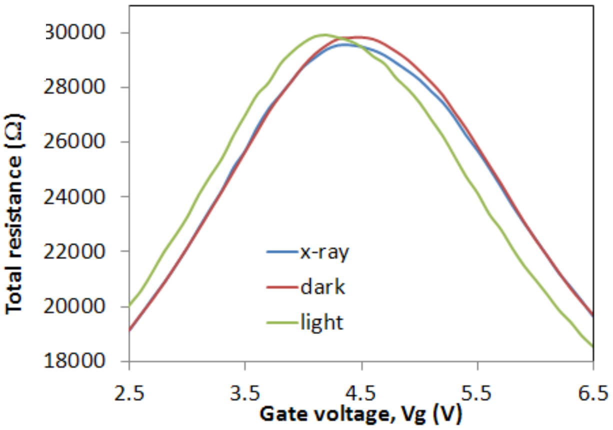

Figure 3.4 Total resistance of the GFET a function of the gate voltage measured in dark, and while exposed to visible light and soft x-rays (10 kV/30 μA).

3.4 Synopsys Sentaurus TCAD simulations

The GFET and GDEPFET semiconductor simulations were made with Sentaurus Device. Also according to the simulations, the capacitance of the substrate is nearly constant, and the small shift detected with the change from dark to strongly illuminated substrate is only 340 mV, which is in full agreement with our experimental results.

The operation in all GDEPFET designs is based on the potential well under the graphene GFET, effectively collecting the photoinduced minority carriers from the full depth of the substrate. These charges induce field into which graphene responds. The GDEPFET structure was optimized on the basis of the principles presented in **RD5.** However, as the thin 50 µm absorber was replaced with thicker 500 µm substrate, the interaction between the neighbouring pixels in the matrix become relevant due to the small size of the pixels (80 µm) compared to the depth. The problem is illustrated in **Figure 3.5**. Even though the potential well (red area between the Source and the Drain) beneath the graphene channel is visible in all the plots, the minority carriers following the field lines marked in the image will not be guided into the well, leading to a high recombination probability in bulk or surfaces instead of collection. This can be corrected by additional Drain and Clear structures on the left side of the Source (see technical notes for details). Also the bias voltage required to guide the minority carriers into the potential well from the full absorber depth is much larger in the 500 µm substrate.

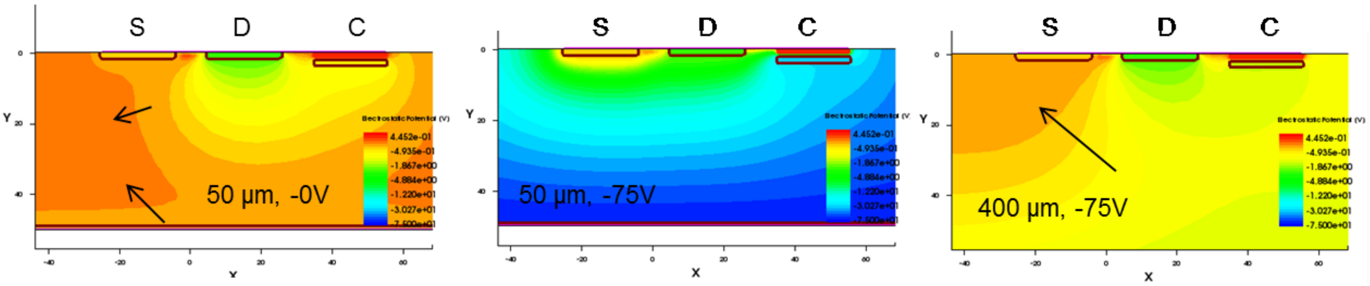

Figure 3.5 The Electrostatic potential to visualize the potential well that forms below the graphene channel. Non-ideal fields are presented with arrows, Source (S), Drain (D) and Clear (C) areas are indicated on top of the structure.

The simulation showed a strong change in the electrostatic potential across the graphene channel (from Source to Drain). As long as this profile is linear, it can be compensated by employing effective gate field in graphene.[11,14] However, providing linearity will be a major challenge for the device design.

The response to the adsorbed ionizing radiation can be estimated by calculating the influence of the charge collected into the potential well to the graphene channel. For 10 keV radiation, in optimal conditions, each photon contributes to a 20 mV change in the electrostatic potential and the potential well is fully compensated already by the charge generated by three photons. This is possible to monitor with graphene FET, but it requires high quality and high transconductance; the corresponding shift of the Dirac peak is on the range on 1–10 mV with thin dielectric (e.g. 10 nm Hf_2O_3).

3.5 Conclusions based on GFET and GDEPFET simulations

For the GFET, the operation requires a substrate that can be made reliably non-conductive also at room temperatures, otherwise the operation can be utilized only at cryogenic temperatures. Also in this case, the issues related to the charge trapping into the Si/SiO_2 interface need to be solved, and this was already the initial triggering problem for the consideration of the GDEPFET structure instead of the simple absorber.

As an alternative device structure we proposed in TN1 (**Figure 3.6**b-c) a dual layer graphene device. There an additional graphene film is placed between the silicon absorber and the gate dielectric to drive the charges from the interface. This film has to be floating during the detection phase for not to influence the electrostatic potential distribution and draining of the charges is done as a clear sequence in between the detection phases. As the role of the additional graphene is only to drain charges, it could be replaced with ultra-shallow (e.g. 2 nm thick) doping layer based on B_2H_3 or BCl_3 process.

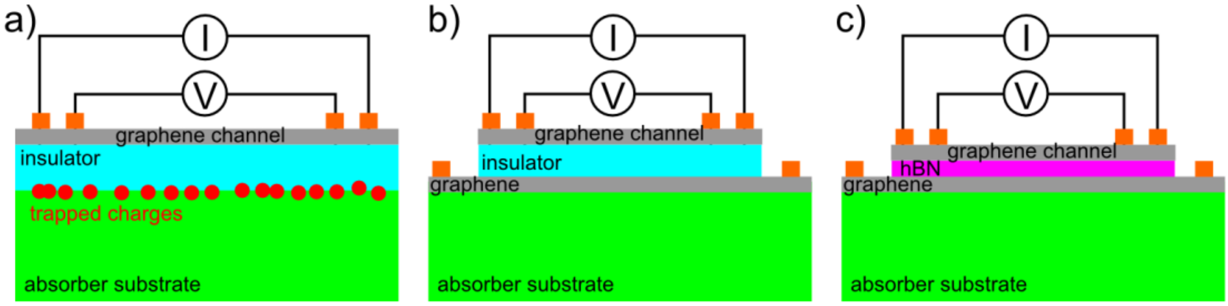

Figure 3.6 a) Illustration of the GFET depicting the trapped charges in the insulator absorber interface. b) As an alternative to near surface quantum confinement by compound semiconductor heterostructures graphene could also be applied in similar manner as conductive drain layer for carriers. c) Instead of utilizing conventional dielectric layer the whole drain-GFET device structure can be manufactured using only 2D materials.

4 Roadmapping and recommendations for graphene based X-ray detectors

GDEPFET structure is an expensive high-end solution, where the readout relies on the accumulated charges in the potential well underneath the graphene channel, instead of the absorber capacitance. This can easily reach very high responsivity, as long as the graphene quality and dielectrics are optimized for high mobility and large gate capacitance to obtain high transconductance. When considering soft X-rays, this design has potential for single photon detection with good energy resolution at room temperature, but it is not suitable for the detection of continuous flux with higher dosage.

4.1 Fabrication, simulation and material specific roadmap for X-ray detectors

In common to all graphene devices, the optimization of the wafer-level graphene processing is they key high performance applications. In the case of X-ray detectors, whatever the structure, the important parameters to optimize in fabrication and design are

1) Transconductance optimization by the optimization of mobility and gate dielectric
2) Field uniformity in graphene gate (signal) to avoid Dirac-peak widening (loss of sensitivity). Metallic gate electrodes are preferred due to their potential uniformity.
3) Top dielectric deposition with high dielectric strength and high uniformity
4) Graphene/dielectric and absorber/dielectric interfaces, to minimize hysteresis
5) Uniformity in doping from bottom- and top dielectrics, to allow the pixel matrix control with equal parameters in each pixel

The optimization of the detector/absorber structure is straightforward semiconductor device design where the amount of efforts required can be easily estimated. Graphene process development and industrial production scale-up, on the other hand, are still in the early phase globally.

From the material point of view, one important aspect in commercialization and applications is the radiation stability of graphene; first considering the radiation induced damage in the actual graphene material and then in the dielectrics and interfaces, which have a strong influence on the electrical properties of the GFETs. These should be studied both structurally (irradiation induced damage in the crystalline structure of graphene; Raman, STM etc.) and from the point of view of device performance (GFET performance changes due to irradiation induced changes in dielectrics, e.g. ionization; experimental and device simulation).

4.2 Commercial aspects and performance of graphene based X-ray detectors

The GDEPFET structure allows single soft X-ray photon detection and energy resolution, but the sensitivity depends on the quality of the graphene and gate dielectrics. The commercialization of such detectors requires massive development of graphene processing technology worldwide, but demonstrators and experimental device optimization are already possible with CVD graphene and ceramic gate dielectrics (e.g. thin Hf_2O_3). Higher sensitivity would be obtained with graphene –hBN stacks, but the commercialization of this structure is even further in the future; however, limited production of high performance devices using dry-transferred *h*BN sandwiched CVD graphene with record high mobility could already be possible for special applications. The performance limits simulated in this project are based on few optimizations considering the overall structure of the detector in 2D. For achieving the true device performance and for further optimization, full 3D model of the DEPFET substrate should be used and the device responsivity should be compared to the more traditional silicon channel. We expect that the GFET structure is probably more responsive to the bottom gating by the charge collecting potential well than the silicon channel. In addition, due to the low noise and high transconductance, graphene may have the potential to bring DEPFET structures into the mainstream of high-performance X-ray detectors.

5 GRAPHENE BASED THZ DETECTION

5.1 Room-temperature detectors for THz regime

Graphene has very high prospects in THz detection and several cryogenic and room-temperature detector concepts have been recently demonstrated. The detection methods in graphene THz detectors, as summarized in Figure 1.1, are **photo-thermoelectric**, **bolometric** and **plasmonic**. Graphene conductivity is strongly frequency dependent enabling pronounced surface plasmonic effects in THz range.

THz **graphene photo-thermoelectric detectors** demonstrated recently[15] utilize embedded thermocouple of Au-Cr dissimilar electrodes. Graphene contacts with different metals produce non-zero thermoelectric response both due to induced asymmetric Fermi energy profile resulting in asymmetric Seebeck coefficient and due to temperature gradient caused by different contact resistances. The first non-optimized detectors showed high photo-thermoelectric response of 100-700 V/W to 2.52 THz waves, yielding lowest optical NEP ~1 nW/rtHz (16 pW/rtHz) referred to incident (absorbed) radiation. Detector noise measurements show Johnson-Nyquist noise floor performance with the response time ~110 ps to 2.52 THz waves. Up to two orders of magnitude improvements of THz sensitivity are expected by using multilayer graphene, coupled THz antenna, tailored plasmonic resonance in graphene and increased thermo-power asymmetry.

Recently demonstrated graphene THz FET (GFET) detectors[16,17,19,20] utilize **plasma wave** rectification phenomena in FETs following Dyakonov and Shur theory for 2D electron gases.[18] In FETs THz detectors, plasma waves in the channel are excited by incoming THz wave modulating the potential difference between gate and source/drain being rectified via non-linear coupling and transfer characteristics in FET. Thus GFET THz detectors exhibit self-mixing (square-law) THz antenna-coupled GFETs with the photovoltage response u proportional to the derivative of the GFET channel conductivity $\sigma(\omega)$ with respect to the gate voltage $V_{G:}$ $u \sim \sigma^{-1}(\omega)\, d\sigma(\omega)/dV_G$. The performance of GFET THz detectors is limited by Johnson-Nyquist noise of the channel resistance.

The non-linearity between the drain and the source can be achieved e.g. by coupling THz antenna with the gate and the source[19]. When plasma wave, excited at the source by incoming THz wave of a f frequency, decays before reaching the drain, the plasma waves are overdamped and allow broadband THz detection. At weakly damped regime $2\pi f\tau$ >~ 1 the momentum relaxation time is long enough to allow for the plasma wave to reach the drain, allowing for a 5–20 times stronger resonantly enhanced response when there is a constructive interference of the plasma waves in the FET channel cavity.

Overdamped plasma wave GFETs have been demonstrated with reported optical NEPs of 0.5 $nW/Hz^{1/2}$ for 0.6 THz single layer GFET[19] and 2 $nW/Hz^{1/2}$ for 0.29-0.38 exfoliated bilayer THz GFETs[20], in a good agreement with Johnson–Nyquist noise floor limits. Higher efficiency requires[20] reaching GFET plasmon resonance conditions by enhancing the carrier mobility, and in the overdamped case, enhancing[20] $d\sigma(\omega)/dV_G$ via a reduction of impurity density or by introducing dual-gate transistor geometries[20].

The performance of the recently lab-demonstrated first graphene based room temperature THz detectors are compared in **Table 5.1** with InP-, GaN-, Si- HEMT and Schottky diode based THz detector technologies.

Table 5.1 Comparison of the State-of-the Art Room temperature THz detectors & the detector measured in this work.

	$NEP_{optical}$	Frequency, [THz]	Antenna
InP HEMT LNA (Northrop Gruman) + zero-bias diode[21]	radiometric NETD ~ 0.46 $K/Hz^{1/2}$ yields 0.6 $pW/Hz^{1/2}$ for 50 GHz bandwidth	0.67	WR-1.5 rectangular waveguide
A-DDG InP HEMT[22]	0.5 $pW/Hz^{1/2}$	0.2	no antenna, 20 x 20 μm^2 area
Zero-bias Schottky diode[23]	< 20 $pW/Hz^{1/2}$	0.05-0.9	sinuous
Si MOSFET 90 nm CMOS[24]	59 / 20 / 63 / 85 / 110 $pW/Hz^{1/2}$	0.22 / 0.59 / 2.52 / 3.11/ 4.25	
GaN HEMT[25]	40 $pW/Hz^{1/2}$	0.9	i-/g- antenna
YBCO resistive bolometer[26]	200 $pW/Hz^{1/2}$	0.1 - 2	spiral
Monolayer graphene FET[19]	515 $pW/Hz^{1/2}$	0.6	bow-tie + hyperhemispherical Si lens
Bilayer graphene FET[16]	2 $nW/Hz^{1/2}$	0.29-0.38	log-periodic circular tooth
Monolayer/Bilayer graphene FET[20]	200 / 30 $nW/Hz^{1/2}$	0.29-0.38	log-periodic circular tooth
Monolayer graphene FET (NEP_{el}) [*This Work*]	300 $nW/Hz^{1/2}$ (*only a single device measured, no fabrication optimization*)	0.65	log-periodic circular tooth
Photothermoelectric[15], AuPd thermocouple on graphene	1 nW / $Hz^{1/2}$ (*ultrafast operation*)	2.52	500x500 μm^2 graphene sheet micro-ribbons area

It is obvious that in order to realize sensitive THz graphene detector one could adapt FET technology and its design approaches in the spirit of 2DEG based HEMT LNA's – (e.g. as in ref.[22]: InP asymmetric dual-grating-gate utilizing rectification from two different plasmonic effects: plasmonic drag and plasmonic ratchet.) – e.g., introducing and tailoring GFET grated-gate designs[27] and THz plasmon Fabry-Perot cavity designs (substrate thickness in a few hundred micron range)[27], and also by graphene-gratings designs. Preserving high mobility of the graphene by keeping it suspended or deposited onto alternative substrates like hexagonal boron nitride represents longer-term development for THz graphene detectors.

5.2 THz GFET Detector demonstration, fabrication and characterization

Graphene field-effect transistors (GFETs) for plasma-wave rectification of THz radiation were fabricated by transferring graphene on the pre-processed HR-Si substrates with sputter-deposited Au tooth log-periodic antenna (**Figure 5.1**). Graphene was first contacted with the antenna (source) and additional pad (drain), and then patterned and etched with oxygen plasma. All of the patterning steps after the graphene transfer were made by e-beam lithography. A 30 nm ALD Al_2O_3 was deposited as the top gate dielectric with the aid of seed layer formed by oxidation of evaporated Al (1 nm). To connect the gate electrode to the right antenna leaf, the Al_2O_3 layer was removed from the contact area and the Ti/Ag top gate metallization was formed by the evaporation and the lift-off. The channel width was 16 µm and the channel length 3 µm, as smaller devices from the first fabrication round had destroyed in analysis. Metal-to-graphene contact areas were 15 x 10 μm^2.

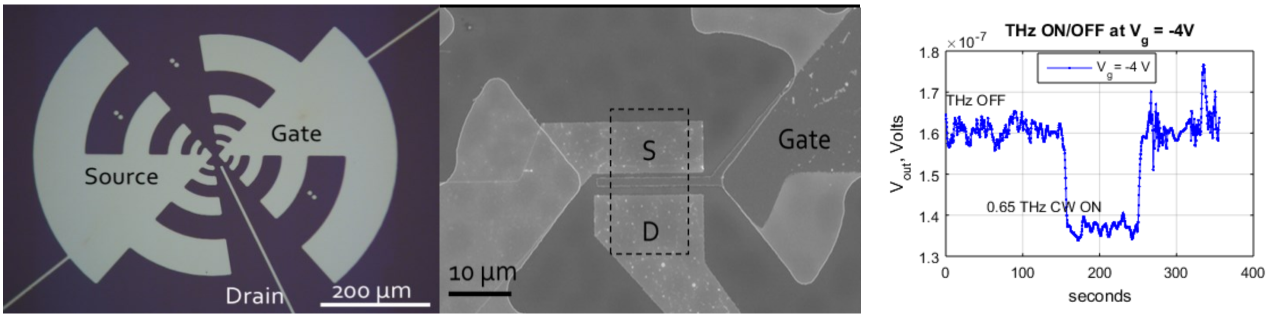

Figure 5.1. a) Optical image of the tooth log-periodic 50 nm Au antenna before the graphene transfer. b) SEM image of the graphene FET THz detector component with the source (S), the drain (D), the gate and the graphene FET channel area (dashed). C) Source-drain voltage vs time (at V_g = -4 V) responding to 0.65 THz CW.

To characterize the detector, the Si hyper-hemispherical lens was attached to the back of THz GFET silicon chip. The GFET was illuminated by the continuous vertically polarized 0.65 THz wave, collimated and focused by two f/3 PTFE lenses. The intensity was mechanically modulated by a chopper at 458 Hz. The GFET photovoltage signal was preamplified by an instrumentation amplifier (gain 10^4) in the voltage differential mode within the 100-1000 Hz bandwidth defined by the built-in first-order RC low- and high-pass amplifier filters. The amplified GFET signal is recorded with a lock-in post-amplifier referred to the chopper modulation frequency.

The measured detector performance results are in a qualitative agreement with the transport models utilized. The responsivity and the upper limit estimate of the NEP are presented together with state of the art THz detectors in Table 5.1, and is at the same order of magnitude as the overdamped plasma-wave based FET-type graphene detectors first demonstrated in publication 2012.[16] The measured sample had a non-optimized THz coupling and low mobility of only 500 cm^2/Vs, which, together with the lack of resources that would have allowed optimizing the device specific processing and design, strongly indicate the potential for significant improvement with more optimized detectors.

Also the basic GFET parameter analysis in **Figure 5.2** strongly indicates the potential for significant performance improvement with higher GFET mobility and transconductance. The implementation of high mobility (above ~5000-10000 cm^2/Vs) THz GFET devices opens possibility to enhance further responsivity dV/dP by introducing gate gratings with sub-µm dimensions for efficient modulation of electron plasma waves along the channel, in analogy with 2DEG FETs (InAlAs/InGaAs/InP). Provided these parameters are achieved and responsivity values dV/dP above 1 kV/W demonstrated @ 1 THz, the THz GFET detector power resolution NEP would yield sub-pW/$Hz^{1/2}$ range at 1 THz (for ~100 Ohm channel resistance), the ultimate benchmark at present.

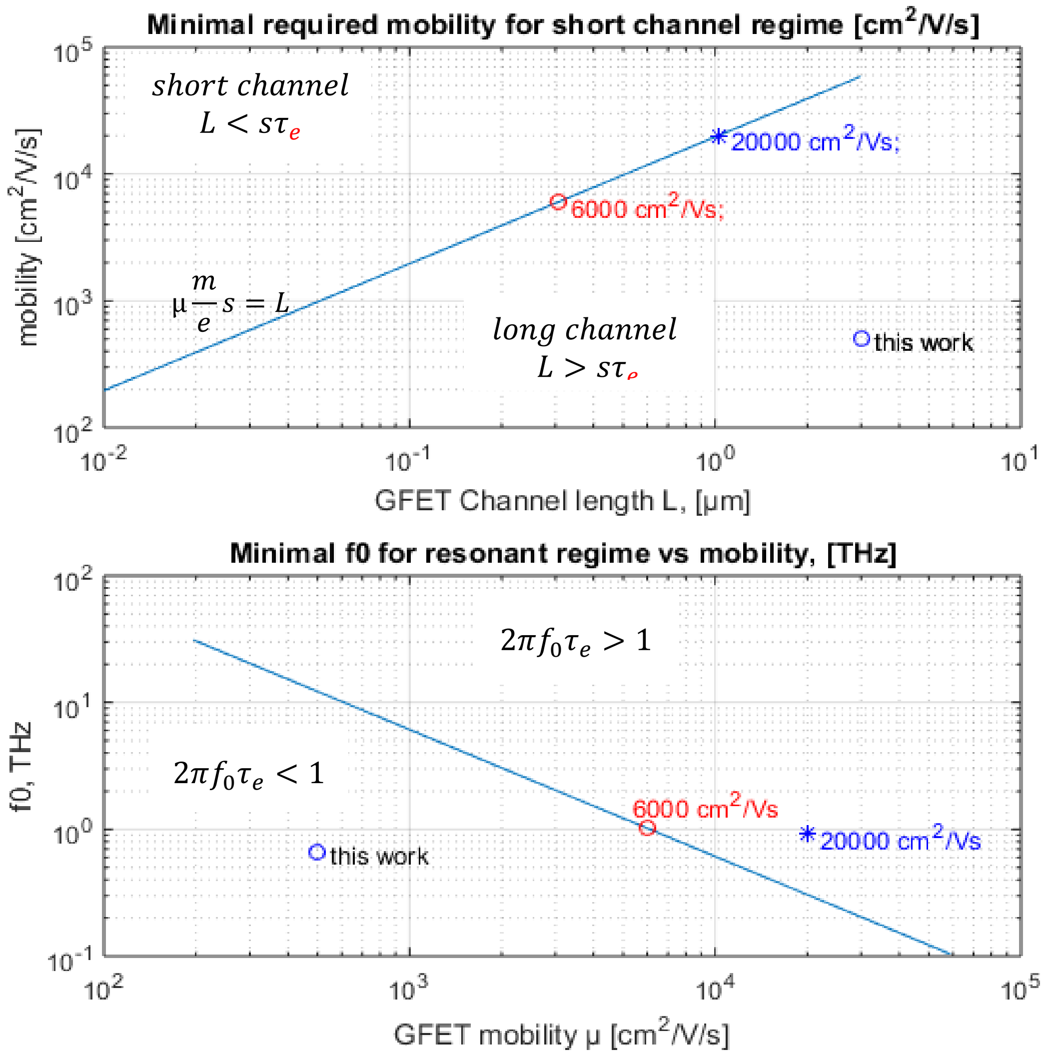

Figure 5.2 Estimated GFET mobility vs GFET (upper panel) and resonant frequency regime vs mobility (lower panel). $\boldsymbol{U} = 1$ V THz induced source-drain DC voltage is assumed. Effective electron mass in graphene m=0.046m$_0$. Graphene plasma wave velocity $\boldsymbol{s} = \sqrt{\boldsymbol{eU/m}}$ ~2e6 m/s.

6 ROADMAPPING AND RECOMMENDATIONS FOR THE GRAPHENE BASED THZ DETECTORS

The successful realization of room-temperature THz radiation detectors would impact in the next generation ultra-fast space communications, space-to-Earth data links, meteorology and climatology, photonics and molecular spectroscopy, surveillance and public security, and medical diagnostics. This is widely considered as one of the most promising application fields of graphene to be developed in the near future.

Currently, proposed technologies for THz imaging in terrestrial applications such as security screening include cryogenic detector systems[36,28,29], and high-end fast semiconducting low-noise amplifiers such as InP HEMTs[30]. Cryogenics sets constraints to the system cost and scalability. Fast semiconductor technology is also currently very expensive with the detector cost of thousands of euros per single detector channel, while an imaging system would benefit from having at least thousands of channels[31]. Thus the primary goal in graphene THz research in terms of utilisation is to develop low-cost imaging systems.

The technology of plasma-based single-layer graphene FET THz detector is currently at the initial level of maturity, where the detector operation is qualitatively understood, and all the parameters can be further tuned to enhance the detector performance. Considering the fabrication and design of the plasma-wave GFET detectors, the following improvements are expected to provide an immediate improvement to the detector performance:

1) Increasing the carrier mobility and decreasing the contact resistance in the GFET devices. Currently this step requires only the device specific (post-) process optimization.
2) The overdamped (non-resonant) plasma-wave detector operation can also be improved by enhancing the gate capacitance per unit area and hence increasing the GFET channel modulation. This can be achieved by using dielectrics with higher dielectric constant (e.g. HfO_2).
3) Design optimization of the channel length to consider the doping induced by the contacts and the area actively modulated by the gate to maximize the channel transconductance in the non-resonant regime. In case the resonant operation regime is achieved, additional design optimization of the plasmonic gate gratings to further enhance the responsivity is feasible. Also the design on the efficient geometry to merge the lithographic antenna and the gate to minimize parasitic effects to be tailored for the desired frequency range.

When considering the potential of graphene in THz detection, it is crucially important to recognize that all of the graphene based THz devices have this far been demonstrated with fairly low mobility graphene, of the order of 2 000 cm^2/Vs. However, the state-of-the art of CVD graphene mobility has very recently been significantly increased by the introduction of dry-transferred hBN encapsulated graphene with record mobilities close to 70 000 cm^2/Vs at room temperature. This material is currently rather widely available for testing purposes and therefore we expected that in the near future the NEP value will outperform standard material based THz detectors. While more than a few years' time is probably required before these materials are industrially available, we can expect CVD graphene with mobility values above 5 000-10 000 cm^2/Vs to be the basis of wafer level processing in the very near future. This already opens the platform for the implementation of high performance graphene THz detectors, mixers, and possibly also low-noise THz amplifiers, in analogy with 2DEG semiconductors.

These components form the basis for the three different THz detection systems:

1) **Non-coherent direct detectors**, as the plasma-wave detector in this project and as the suggested graphene membrane based bolometer with extremely low thermal mass. The commercial state-of-the-art components in this category are the zero bias diodes (ZBD) by Virginia Diodes (US) that have NEP of 3-13 $pW/Hz^{0.5}$ across the 0.1 – 2 THz frequency range with 50-600 GHz bandwidth and a typical price tag of few k€/component.
    - Considering the current state-of-the-art with relatively low-mobility graphene (NEP 500 $pW/Hz^{0.5}$), better optimized plasma-wave based overdamped (wide bandwidth) devices will definitely have a chance to compete with price and performance.

    - The NEP predicted for graphene membrane based room –temperature bolometers is highly competitive.
    - In resonant mode the plasma-wave GFET has high sensitivity and narrow spectral range which could facilitate low-cost active spectroscopy when combined with broad band source.
2) **Downconversion devices** (e.g. mixers), such as Virginia Diode (US) with commercial noise temperature of 1000-15000 K and <10 dB conversion loss of at the 0.22 – 0.65 THz range typically used for active imaging. These devices are also used in THz spectroscopy and non-destructive testing & evaluation (NDT, NDE), duo to the high spectral resolution obtained by coherent source-detector combination (e.g. Teraview).
    - Graphene mixers have already been realized for sub-THz region, and the activities on THz range are intense. Demonstration of THz mixing would be of extremely high impact both scientifically and technologically.
3) **Amplifying devices** combined with downconversion components, such as the Northorp-Grumman amplifiers with noise figure of 8 dB (corresponding to NEP of 4 fW/Hz$^{0.5}$ with the reported 40 GHz bandwidth).
    - Graphene based THz amplifiers are currently under theoretical investigation and several possible (usually plasmonics) structures have been proposed.
    - For downconversion electronics, see above.

For active THz applications, such as gas spectroscopy and active imaging, coherent THz detection is preferred as the coherent detection allows accurate analysis with much higher NEP. The coherent detection scheme relies on a combination of a coherently coupled THz source and mixer-type detector, typically including also amplifier to enhance the detected signal.

THz sources and other devices beyond non-coherent detection have been studied theoretically already from the early 2000s, including e.g. coherent sources based on negative resistance achievable at THz frequencies[32] in 2007 and more recently introduced nanopatterned graphene/*h*BN/graphene heterostructures.[33] Experimentally this field is still unexplored, consisting of a few demonstrations of optically pumped THz emission and a simple antenna-coupled field-effect transistor design[34] in 2015. Considering mixers and other components for THz manipulation, the situation is rather similar.

On this basis, **the recommendation** in advancing the graphene based THz technology is **to focus on plasma-wave detectors that allow both direct (incoherent) and coherent detection**. The optimization and careful analysis of the detector performance with respect to the structure and graphene properties in the coherent and non-coherent mode should be examined simultaneously and used for the construction of better models for the development of both detection modes. As a parallel method, the highly sensitive room-temperature bolometers utilising the ultra-low heat capacity of graphene membranes could be addressed theoretically and experimentally.

The ultimate question is whether, with graphene based devices, one can reach the sensitivity levels typically characterised by NEP of the order of 0.01–0.1 pW/Hz$^{1/2}$. This is the typical minimum requirement of passive radiometric imaging of room temperature targets and leads to a radiometric object contrast below one Kelvin in a typical imaging setup using the imaging bandwidth from a few tens of GHz to few hundred GHz.

The coherent detector technology is relevant for active imaging and spectroscopy and could rely on graphene based mixers as receivers. The benefit in using coherent receivers is that the intrinsic sensitivity requirement for nonlinear devices is typically less restricting than in the incoherent mode of operation: a receiver with a noise temperature in the order of 1000 K can yield a radiometric contrast below 1 K. The trade-off is that in addition to the sensor one needs the source to act as the local oscillator for the receiver. For this end it would be beneficial to study the usefulness of graphene based devices as sources, considering the feasibility of both optically and electrically pumped systems.

The work towards higher TRL levels in specific applications areas can also be defined via the required performance and integration targets for graphene devices:

1) Security surveillance, passive THz imaging:
    a. Detector operation range 0.1 – 1 THz, multiband preferred
        - Non-resonant mode in plasma-wave GFET detector, bolometer
    b. Typical speed/sensitivity requirement* 60 Hz FPA frame rate with 10 $\mathrm{fW/Hz}^{0.5}$
        - Requires significant improvement in GFET NEP, may be somewhat compensated*
    c. Integration of kpixel focal plane array into THz cameras[31]
2) Radar technology for active safety surveillance; NDT and NDE
    a. Detector operation range 0.1 – 1…1.5 THz
    b. Detector speed/sensitivity requirements depend on the source*
        - Graphene based THz mixer
    c. Integration into an imaging radar for non-destructive imaging[35]
3) Gas and molecular spectroscopy
    a. The detector operation range 0.01 – 5 THz (gases), 0.1 – 1.5 THz (solids)
        - Resonant mode plasma-wave GFET, with bandwidth < 10% of the frequency
        - Coherent tunable source and mixer

*The utilization of the high detection speed of GFET type detectors (response times of 30–110 ps demonstrated) in graphene allows further averaging that efficiently reduces the NEP requirement compared to conventional THz detectors.

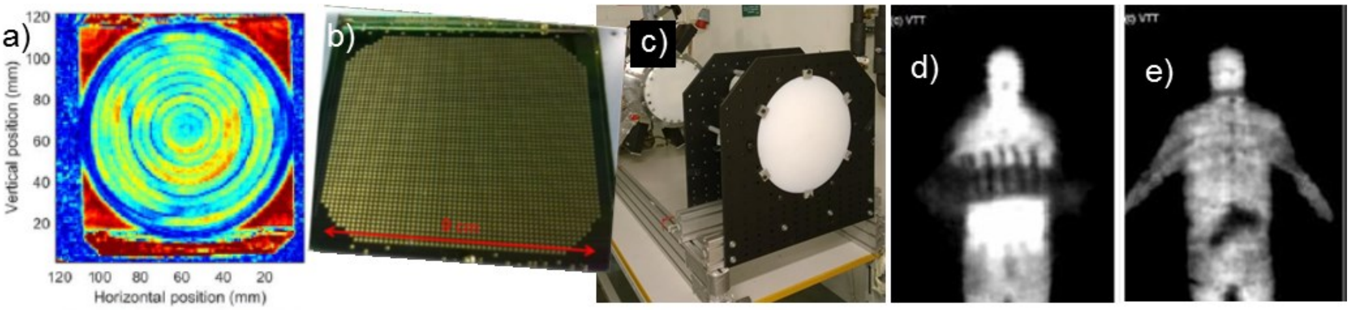

Figure 6.1 THz detector systems demonstrated at VTT. a) Non-destructive imaging by frequency modulated continuous wave radar. Image of buried structures in a plastic container.[35] b) Kinetic inductance bolometer focal plane array for sub-mm radiometric imaging c) integrated with lens system.[31] C) Passive THz imaging screen shots from 0.6 THz cryogenic bolometer array fabricated at VTT, revealing hidden explosives d) and a hand gun e) in safety surveillance demonstrator.[36]

6.1 Commercial aspects of graphene based THz detectors

The current technology readiness level and the performance level of THz graphene detectors are still low if compared to the state of the art III-V semiconductor based THz detectors. However, the first demonstrations of graphene based THz detection are still very recent, and several device concepts show high theoretical performance relying on the ideal case of ultra-high graphene mobility, whereas demonstrated modest experimental NEP values down to below ~1 nW/Hz$^{0.5}$ are in line with the predictions for low mobility values. There is still some uncertainty in some of the theoretical aspects that can be seen as a risk for achieving the high performance, but on the other hand, they can also be seen as challenges to overcome in order to utilize the full power of graphene in THz detection.

At the moment it seems clear that graphene will offer relatively low-cost fabrication of very simple devices capable of fast THz detection in room temperature, the only question is in the sensitivity that will define the range of applications. Also the market of the room-temperature THz detectors is by no means mature and the need for fast and sensitive detectors is intense. High performance graphene devices will have an extensive commercial and technological impact in many different fields ranging from security surveillance to molecular spectroscopy and beyond. Therefore the theoretical and experimental research should move together (or in advance) of the technological progress in graphene processing.

Research Documents

N	Reference	Title	Author	Date
RD1	IEEE, Trans. on Nanotech. **11** (3)	Graphene Field-Effect Transistors on Undoped Semiconductor Substrates for Radiation Detection http://ieeexplore.ieee.org/xpl/periodicals.jsp	M. Foxe *et al.*	2012
RD2	IEEE Nucl. Sci. Symp. Conf. Rec., 23 - 29 Oct.	Graphene Field Effect Transistor as Radiation Sensor http://ieeexplore.ieee.org/xpl/periodicals.jsp	A. Patil *et al.*	2011
RD3	IEEE Electron Device Letts. 31 (9)	Graphene-Based Ambipolar RF Mixers http://ieeexplore.ieee.org/xpl/periodicals.jsp	H. Wang *et al.*	2010
RD4	IEEE Nucl. Sci. Symp. Conf. Rec., Orlando, FL, Oct. 24 - Nov. 1	Detection of Ionizing Radiation Using Graphene Field Effect Transistors http://ieeexplore.ieee.org/xpl/periodicals.jsp	M. Foxe *et al.*	2009
RD5	IEEE Nucl. Sci. Symp. Conf. Rec., 23 - 29 Oct.	Design and Simulation of a Graphene DEPFET Detector http://ieeexplore.ieee.org/xpl/periodicals.jsp	O. Koybasi *et al.*	2011
RD6	Nucl. Instr. and Meth. A253 (3)	New detector concepts http://www.journals.elsevier.com/nuclearinstruments-and-methods-in-physicsresearch-section-a-acceleratorsspectrometers-detectors-and-associatedequipment/	J. Kemmer, G. Lutz	1987
RD7	Proc. IEEE Nucl. Sci. Symp. Conf. Rec., 23 – 29 Oct.	Graphene-based neutron detectors http://ieeexplore.ieee.org/xpl/periodicals.jsp	M. Foxe *et al.*	2011

REFERENCES

---

[1] F. Xia., T. Mueller, Y. Lin, A. Valdes-Garcia and P. Avouris, "Ultrafast graphene photodetector", Nature Nanotech. 4, 838 – 843 (2009).

[2] F. Koppens, T. Mueller, P. Avouris, A. Ferrari, M. Vitiello and M. Polini, "Photodetectors based on graphene, other two-dimensional materials and hybrid systems", Nature Nanotechnology **9**, 780 (2014).

[3] E. Peters, E. Lee, M. Burghard and K. Kern, "*Gate dependent photocurrents at a graphene p–n junction*", Appl. Phys. Lett. **97**, 193102 (2010); G. Rao, M. Freitag, H.-Y. Chiu, R. Sundaram and P. Avouris, "*Raman and photocurrent imaging of electrical stress-induced p–n junctions in graphene*", ACS Nano **5**, 5848–5854 (2011); T. Mueller, F. Xia, M. Freitag, J. Tsang and P. Avouris, "*Role of contacts in graphene transistors: A scanning photocurrent study*", Phys. Rev. B **79**, 245430 (2009); M. Freitag, T. Low, F. Xia and P. Avouris, "*Photoconductivity of biased graphene*", Nature Photon. **7**, 53–59 (2012).

[4] R. Kim, V. Perebeinos and P. Avouris, "*Relaxation of optically excited carriers in graphene*", Phys. Rev. B **84**, 075449 (2011); E. Malic, T. Winzer, E. Bobkin and A. Knorr, "*Microscopic theory of absorption and ultrafast many-particle kinetics in graphene*", Phys. Rev. B **84**, 205406 (2011).

[5] D. Brida, et al. "*Ultrafast collinear scattering and carrier multiplication in graphene*", Nature Commun. **4**, 1987 (2013); E. Malic, T. Winzer, E. Bobkin & A. Knorr, "*Microscopic theory of absorption and ultrafast many-particle kinetics in graphene*", Phys. Rev. B **84**, 205406 (2011); T. Winzer, A. Knorr & E. Malic, "*Carrier multiplication in graphene*", Nano Lett. **10**, 4839–4843 (2010).

[6] C. Liu, Y. Chanh, T. Norris and Z. Zhong, "*Graphene photodetectors with ultra-broadband and high responsivity at room temperature*", Nature Nanotech. **9**, 273 – 278 (2014).

[7] Y. Liu, R. Cheng, L. Liao, H. Zhou, J. Bai, G. Liu, L. Liu, Y. Huang and X. Duan, "*Plasmon resonance enhanced multicolour photodetection by graphene*", Nature Comm. **2**, 579, (2011).

[8] G. Konstantatos, M. Badioli, L. Gaudreau, J. Osmond, M. Bernechea, F. P. Garcia de Arquer, F. Gatti and F. Koppens, "*Hybrid graphene–quantum dot phototransistors with ultrahigh gain*", Nature Nanotech. **7**, 363–368 (2012).

[9] T. Winzer, A. Knorr, E. Malic, "*Carrier Multiplication in Graphene*", Nano Lett. **10**, 4839 (2010).

[10] C. Liu, Y. Chanh, T. Norris and Z. Zhong, "*Graphene photodetectors with ultra-broadband and high responsivity at room temperature*", Nature Nanotech. **9**, 273 – 278 (2014).

[11] W. Kim, C. Li, N. Chekurov, S. Arpiainen, D. Akinwande, H. Lipsanen, J. Riikonen, "*All-Graphene Three-Terminal Thin-Film Transistors as Rectifiers and Inverters for Integrated Circuits*", ACS Nano **9** (6), 56666 (2015).

[12] W. de Heer, C. Berger, X. Wu, P. First, E. Conrad, X. Li, T. Li, M. Sprinkle, J. Hass, M. Sadowski, M. Potemski and G. Martinez, "*Epitaxial graphene*", Solid State Communications **143**, 92 (2007).

[13] O. Koybasi, E. Cazalas, I. Childres, I. Jovanovic, and Y.P. Chen, "*Detection of light, X-rays, and gamma rays using graphene field effect transistors fabricated on SiC, CdTe, and AlGaAs/GaAs substrates*", Nuclear Science Symposium and Medical Imaging Conference (NSS/MIC), 2013.

[14] Y. Wu, D. Farmer, W. Zhu, S.-J. Han, C. Dimitrakopoulos, A. Bol, P. Avouris, and Y.-M. Lin, "*Three-Terminal Graphene Negative Differential Resistance Devices*", ACS Nano **6** (3), 2610 (2012).

[15] X. Cai, A. Sushkov, R. Suess, M. Jadidi, G. Jenkins, L. Nyakiti, R. Myers-Ward, S. Li, J. Yan, K. Gaskill, T. Murphy, D. Drew and M. Fuhrer, "*Sensitive room-temperature terahertz detection via the photothermoelectric effect in graphene*", Nature Nanotech. **9**, 814 (2014).

[16] L. Vicarelli, M. Vitiello, D. Lombardo, A. Ferrari, W. Knap, M. Polini, V. Pellegrini and A. Tredicucci, "*Graphene field-effect transistors as room-temperature terahertz detectors*", Nature Mat. **11**, 865 – 871 (2012).

---

[17] A. Tomadin, A. Tredicucci, V. Pellegrini, M. Vitiello and M. Polini, “*Photocurrent-based detection of terahertz radiation in graphene*”, Appl. Phys. Lett. **103**, 211120 (2013).

[18] M. Dyakonov, M. Shur, “Shallow water analogy for a ballistic field effect transistor: New mechanism of plasma wave generation by dc current”, Phys. Rev. Lett. **71**, 2465–2468 (1993); M. Dyakonov, M. Shur, “*Detection, mixing, and frequency multiplication of terahertz radiation by two-dimensional electronic fluid*”, IEEE Trans. Electron Dev. **43**, 380–387 (1996).

[19] A. Zak *et.al.*, “*Antenna-integrated 0.6 THz FET Direct Detectors based on CVD graphene*”, Nano Lett. 2014, 14, 5834.

[20] D. Spirito, D. Coquillat, S. Bonis, A. Lombardo, M. Bruna, A. Ferrari, V. Pellegrini, A. Tridicucci, W. Knap and M. Vitiello, “*High performance bilayer-graphene terahertz detectors*”, Apll. Phys. Lett. 104, 061111 (2014).

[21] E. N. Grossman et. al., ”*Passive 670 GHz imaigng with uncooled LNA HEMT coupled to zero-bias diodes*”. *Proc. SPIE* 9078, Passive and Active Millimeter-Wave Imaging XVII, 907809 (2014).

[22] Y. Kurita et.al., “*Ultrahigh sensitive sub-terahertz detection by InP-based asymmetric dual-grating-gate high-electron-mobility transistors and their broadband characteristics*”, Appl. Phys. Lett. 104, 251114 (2014).

[23] L. Liu, J. Hesler, H. Xu, A. Lichtenberger, R. Weikle, II IEEE Microwave Wireless Compon. Lett. 9, 504 (2010).

[24] H. Sherry et al. “*In Lens-integrated THz imaging in 65nm CMOS technologies*”, RFIC 2011: IEEE Radio Frequency Integrated Circuits Symposium, Baltimore, MD, June 5−7, 2011; IEEE: New York, 1−4; M. Bauer et al., Opt. Express 22, 19235 (2014).

[25] Sun, J. D.; Sun, Y. F.; Wu, D. M.; Cai, Y.; Qin, H.; Zhang, B. S. Appl. Phys. Lett. 2012, 100, 013506.

[26] S. Bevilacqua, S. Cherednichenko, “*Fast room temperature THz bolometers*”, Proceedings of the 38th International Conference on Infrared, Millimeter, and Terahertz Waves (IRMMW-THz), Mainz, Germany, Sept. 1–6, 2013

[27] Y. Bo et. al., “*Tunable THz plasmon in grating-gate coupled graphene with a resonant cavity*”, Chin. Phys. B 24, 1(2015) 015203.

[28] A. Timofeev *et al.*, "*Sub-mm wave kinetic inductance bolometer on free standing nanomembranes*", Supercond. Sci. Technol . **27**, 025002, (2014).

[29] E. Heinz *et al*, "*Toward high-sensitivity and high-resolution submillimeter-wave…", Opt. Eng.* **50**, 113204 (2011).

[30] E. Grossman *et al.*, "*Terahertz active and passive imaging", Proc. 8th EuCAP, 2221 (2014).*

[31] J. Hassel *et al.* "*Bolometric kinetic inductance detector technology for submillimeter radiometric imaging*", Proc. SPIE **9651**, 96510G-1 (2015).

[32] M. Ryzhii, V. Ryzhii, "*Injection and Population Inversion in Electrically Induced p–n Junction…*", JJAP 46, L151 (2007).

[33] S. Mikhailov, "*Graphene-based voltage tunable coherent terahertz emitter*", Phys. Rev. B **87** (11), 115405 (2013).

[34] J. Tong *et al.*, "Antenna Enhanced Graphene THz Emitter and Detector", Nano Letters 15 (8), 5295 (2015)

[35] J. Luomahaara *et al.*, “Characterization of sub-range-bin spatial features with frequency modulated continuous wave radar operated at 650 GHz”, Global Symposium of Millimeter Waves (GSMM) and ESA Workshop on Millimetre-Wave Technology and Applications (2016).

[36] A. Luukkanen *et al.*, "*Measured performance of a high resolution passive video-rate submillimeter-wave imaging system demonstrator for stand-off imaging*", Proc. of SPIE **8362**, 836209 (2012).